International Journal of Minerals, Metallurgy and Materials
Volume 20, Number 12, December 2013, Page 1134
DOI: 10.1007/s12613-013-0846-9

Non-isothermal reduction kinetics of titanomagnetite by hydrogen

Jie Dang[1,2)], *Guo-hua Zhang*[1,2)], *Xiao-jun Hu*[1,2)], *and Kuo-chih Chou*[1,2)]

1) State Key Laboratory of Advanced Metallurgy, University of Science and Technology Beijing, Beijing 100083, China.
2) School of Metallurgical and Ecological Engineering, University of Science and Technology Beijing, Beijing 100083, China.

(Received: 29 March 2013; revised: 19 July 2013; accepted: 23 July 2013)

Abstract: Reduction of titanomagnetite (TTM) powders by H_2-Ar gas mixtures was investigated under a non-isothermal condition by using a thermogravimetric analysis system. It was found that non-isothermal reduction of TTM proceeded via a dual-reaction mechanism. The first reaction was reduction of TTM to wüstite and ilmenite, whereas the second one was reduction of wüstite and ilmenite to iron and titanium dioxide. By using a new model for the dual reactions, which was in an analytical form and incorporated different variables, such as time, temperature, particle size, and hydrogen partial pressure, rate-controlling steps for the dual reactions were obtained with the apparent activation energies calculated to be 90-98 and 115-132 kJ/mol for the first and second reactions, respectively.

Keywords: titanomagnetite; ore reduction; hydrogen; reaction kinetics

1. Introduction

As mentioned in the previous work [1], the direct reduction process, especially gas-based reduction, is being actively pursued because coke and high-grade mineral resources are getting exhausted. Furthermore, coking and sintering involved in the traditional blast furnace ironmaking process can lead to high cost and serious environmental problems. As a high-temperature metallurgical process based on carbon, a great amount of CO_2 and many kinds of pollutants such as oxysulfide, oxynitride, and dusts are generated [2].

Titanium-containing iron ores from New Zealand, which are mainly composed of titanomagnetite (TTM), have been becoming an alternative source of iron for their large deposit and lower price than conventional hematite iron ores [3]. However, because of the strong influence of titanium on the reduction mechanism and rate of iron oxides in TTM ores, complete reduction of TTM by carbon monoxide or carbon requires long time and high temperature as well as high reducing potential [4-5]. Hydrogen, as a clean energy, can be used as a reducing gas in production of iron [6] and other metals, such as copper [7] and tungsten [8]. Therefore, reducing TTM by hydrogen seems to be a promising method to obtain direct reduction iron at low temperature.

In literatures, many excellent researches on hydrogen reduction of titanium-containing iron ores (ilmenite) have been published [9-12]. However, researches on TTM reduction by hydrogen are very limited, except some works that are focused on isothermal reduction [1,13]. Because during the practical production process, iron ore reduction is not always under a constant temperature condition from the beginning to the end but under a variable temperature condition, it is necessary to study the kinetics of non-isothermal reduction of TTM by hydrogen.

2. Material and experimental procedure

2.1. Material

The chemical compositions of TTM ores from New Zealand are presented in Table 1. X-ray diffraction (XRD) analysis (Fig. 1) indicates that TTM ores are mainly composed of a solid solution $Fe_{3-x}Ti_xO_4 (x \approx 0.27)$ of magnetite (Fe_3O_4) and ülvospinel (Fe_2TiO_4). The ore particle size was screened to be in the range of 150-160 μm. The specific surface area was determined as 0.8 m^2/g by using the BET method on an Autosorb-1C Quanta chrome analyzer.

2.2. Experimental procedure

The weight change of TTM powders during reduction

Corresponding author: Guo-hua Zhang E-mail: ghzhang_ustb@163.com

Table 1. Chemical compositions of TTM powder wt%

Total Fe	CaO	MgO	Al_2O_3	SiO_2	TiO_2
56.9	0.17	3.23	2.99	3.78	9.01

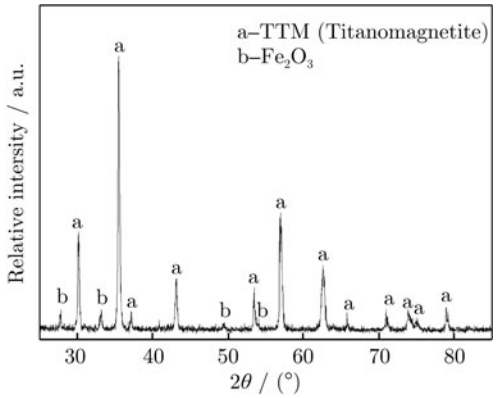

Fig. 1. XRD pattern of TTM.

was monitored using a thermal analysis system (HCT-2, Beijing Hengjiu Instrument Ltd., Beijing, China). Thermogravimetric microbalance was sensitive within ±0.1 μg. Experimental setup and the schematic of the reactor are presented elsewhere [1]. In each experimental run, the powders of about 100 mg were weighted and put into an alumina crucible. When the crucible with a sample was placed in the furnace, argon was introduced into the system to drive air out. The furnace was first heated from room temperature to 973 K at a heating rate of 20 K/min in argon atmosphere, and then the rate of heating was changed to 8, 10, 12, or 14 K/min, respectively, and at the same time, argon was switched to hydrogen or hydrogen-argon gas mixtures to start the reaction. After a predetermined time, the reducing gas was changed to argon again, and the sample was cooled to room temperature for XRD analysis.

Hydrogen and argon used in the experiments were in high purity ($< 5 \times 10^{-6}$ O_2). The flow rates of gases were controlled by gas flow controllers (Alicant, Model MC-500SCCM-D). In all of the experimental runs, a constant flow rate of 50 mL/min was remained during the reduction. This level was found to be sufficient for diminishing the resistance of diffusion in the gas-boundary layer around the sample. XRD (Model, TTRIII, Japan) measurements were carried out for samples. The morphologies of the samples were observed by using a scanning electron microscope (SEM, Model S250MK3, Cambridge, UK).

3. Results and discussion

At temperatures above 843 K, the existence of wüstite as an intermediate phase in the reduction course of magnetite has been proven by Jozwiak *et al.* [14]. Also, it has been found that TTM reduction was started from magnetite in the magnetite-ülvospinel solid solution, which was reduced to wüstite [1,4]. Therefore, the main reduction path will be approximately expressed as follows:

$$\text{TTM} \rightarrow \text{wüstite} \rightarrow \text{iron} \qquad (1)$$

The extent of reduction was calculated as a mass fraction of oxygen removed during reduction to that in iron oxides. The extent of reduction was calculated by

$$R = \frac{w_t}{w} \qquad (2)$$

where w_t is the mass loss of the sample after time t and w is the theoretical total mass loss of the sample. If TTM was reduced completely, w is calculated to be $0.2053w_0$ (according to the mass of oxygen combined with iron), in which w_0 is the initial mass of TTM powders.

3.1. Influence of heating rate

The experiments of non-isothermal reduction at different heating rates were carried out in order to interpret the reaction mechanism and to optimize the kinetic parameters by the following kinetic analysis. Fig. 2 shows the variations of reduction extent with temperature at four different heating rates, namely, 8, 10, 12, and 14 K/min (from 973 to 1300 K). It is indicated in Fig. 2(a) that the rate of reduction reaction became fast at around 1000 K, although the reaction temperature was slightly different at different heating rates, and in the experimental range, all of the non-isothermal reduction experiments were finished

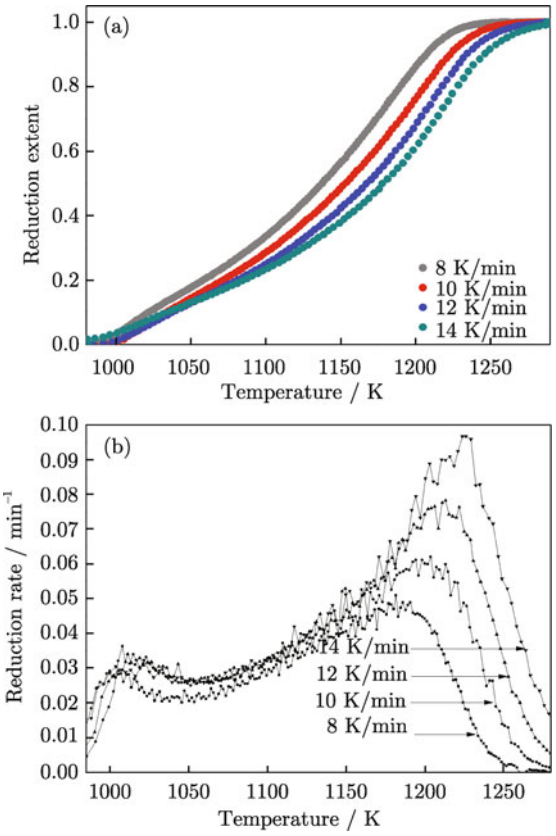

Fig. 2. Non-isothermal reduction curves: (a) reduction extent versus temperature; (b) reduction rate versus temperature.

when the temperature rose to 1290 K. From Fig. 2(b), it can be obtained that a high heating rate could lead to a high reaction rate and the maximum rate appeared at 1191, 1204, 1213, and 1227 K for the heating rates of 8, 10, 12, and 14 K/min, respectively. The small reaction rate at low temperature was due to the relatively small reduction rate constant but at high temperature was because of the depletion of oxygen combined with iron and the large diffusion resistance of hydrogen in the product layer. The highest reduction rate occurred at a temperature at which both the reduction rate constant and the iron oxide concentrations were at high levels as well as the resistance of diffusion was at a small level.

3.2. Influence of hydrogen partial pressure

The influence of hydrogen partial pressure on the non-isothermal reduction of TTM was studied by reduction of TTM powders in H_2-Ar gas mixtures. The ratio of P_{H2} to $P_{H2} + P_{Ar}$ varied in the range of 0.5-1 (P was the partial pressure). The reduction curves are presented in Fig. 3, which shows clearly that the increase of hydrogen partial pressure caused an increase of reduction extent, which was because that the increase of hydrogen partial pressure resulted in the increase of reaction rate. In the temperature range of 1100-1250 K, there was a sharp increase of reduction rate as the hydrogen partial pressure increasing. Also, it was found that the increase of hydrogen content from 50vol% to 70vol% and from 70vol% to 90vol% caused visible increases of reduction rate. However, a further increase from 90vol% to 100vol% had a relatively slight effect. The reason causing the above phenomena should be that the reaction rate was not linearly related to hydrogen partial pressure.

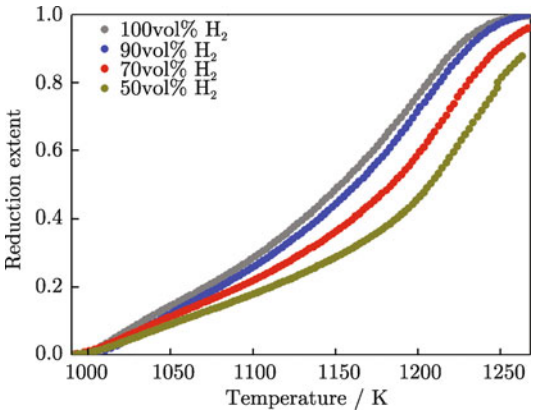

Fig. 3. Non-isothermal reduction of TTM powders in different reducing atmospheres.

3.3. Phase evolution during non-isothermal reduction of TTM

Phase evolution during the non-isothermal reduction of TTM at a heating rate of 10 K/min is shown in Fig. 4. Phases in samples based on Fig. 4 are presented in Table 2. It can be seen that the intermediate phases (wüstite and ilmenite) and the final products (iron and titanium dioxide) were detected in the course of reduction. When the temperature achieved 1290 K, the peaks of metallic iron became dominant in XRD patterns, and some traces of titanium dioxide peaks also appeared.

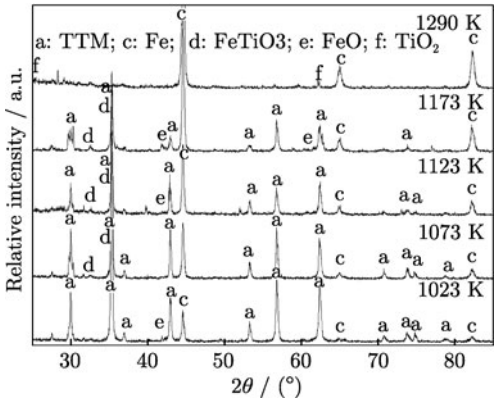

Fig. 4. Phase evolution during the non-isothermal reduction of TTM by hydrogen.

Table 2. Phase evolution during TTM reduction by hydrogen (based on XRD analyses; Fig. 4)

Temperature / K	Phases identified by XRD
1023	TTM, Fe, FeO
1073	TTM, Fe, $FeTiO_3$
1123	TTM, Fe, FeO, $FeTiO_3$
1173	TTM, Fe, FeO, $FeTiO_3$
1290	Fe, TiO_2

According to above analyses, it can be concluded that magnetite in the TTM was first reduced to wüstite and thereafter to iron, whereas ülvospinel was first reduced to iron and ilmenite and then to iron and TiO_2. Furthermore, the two reactions (reduction of TTM to wüstite and ilmenite as well as reduction of wüstite and ilmenite to iron and titanium dioxide) proceeded simultaneously from the beginning to the end, which was similar to TTM reduction under the isothermal condition [1]. Therefore, the reduction path of TTM under the experimental condition can be expressed as follows.

The first reaction:

$$Fe_{3-x}Ti_xO_4 + (1-x)H_2 = (3-2x)FeO + xFeTiO_3 + (1-x)H_2O \quad (3)$$

The second reaction:

$$(3-2x)FeO + xFeTiO_3 + (3-x)H_2 = (3-x)Fe + xTiO_2 + (3-x)H_2O \quad (4)$$

3.4. SEM analysis

Figs. 5(a) and 5(b) present the SEM images of the raw sample and the sample reduced completely under the non-

isothermal condition, respectively. It can be obtained that the raw TTM powders were nonporous. Therefore, hydrogen gas should first diffuse to the surface of TTM powders and react from the outer surface to the inner part. However, the product layer was porous and many pores were formed. This volume decrease was due to oxygen removing during the reduction process, which was beneficial for H_2 and the product water vapor diffusion.

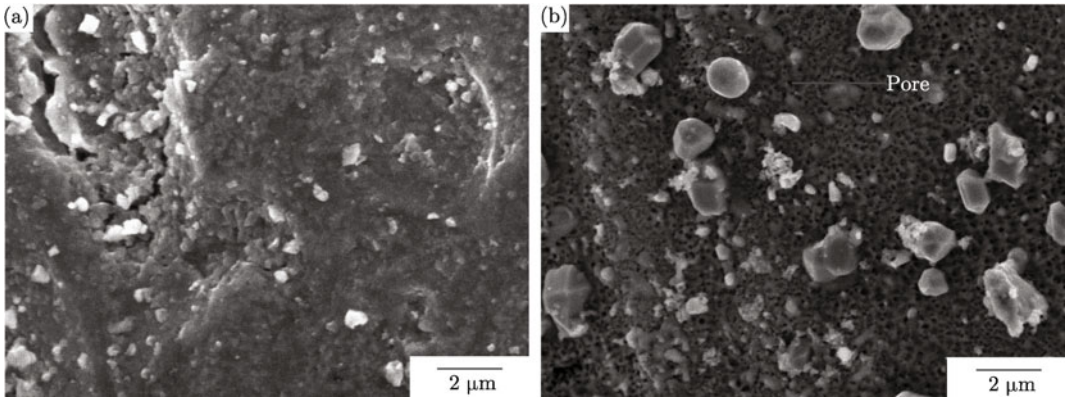

Fig. 5. Morphologies of samples: (a) raw sample; (b) completely reduced sample.

3.5. Reaction kinetics

3.5.1 Theory

According to the results of XRD analyses, it can be concluded that the dual reactions shown in Eqs. (3) and (4) occurred simultaneously. Thus, the reduction mechanism can be described as the one that the reduction proceeds first between TTM and H_2 at the outer surface of the powders with the forming of wüstite and ilmenite. Once wüstite and ilmenite are formed, the second reaction will proceed immediately. Therefore, it can be assumed that TTM reduction proceeds topo-chemically and two reaction fronts exist corresponding to reactions (3) and (4) as shown in Fig. 6.

As clearly shown in Fig. 5(b), many pores formed in the outer product layer, which would be beneficial for hydrogen and water vapor diffusion. Thus, it may be reasonable to assume that the second reaction is not controlled by the diffusion of gaseous species through the product layer but most likely controlled by the chemical reaction at the interface II (Fig. 6). However, for the first reaction, due to the forming and growing of two product layers, the diffusion of gaseous species through the wüstite and ilmenite layer will become relatively slow. Therefore, the diffusion of gaseous species in the product layer may become the rate-controlling step in the reduction of TTM to wüstite and ilmenite.

Based on above analyses, the dual-reaction kinetic model [15-16] can be used to describe the reduction behavior of TTM. The formula for describing the reduction extent ξ with temperature T, hydrogen partial pressure P_{H_2}, and other variables has been deduced as follows [15]:

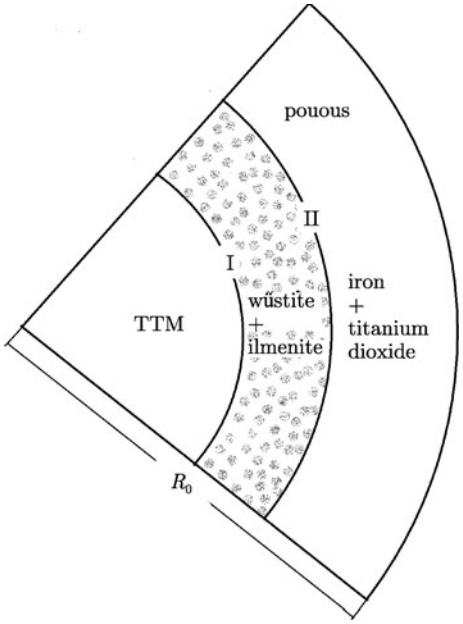

Fig. 6. Interface progressions for TTM reduced by hydrogen.

$$\xi = 1 - \alpha_1 \left[1 - \sqrt{\frac{2K_{\mathrm{H}}^{0\beta} D_{\mathrm{H}}^{0} \left(\sqrt{P_{\mathrm{H_2}}} - \sqrt{P_{\mathrm{H_2}}^{\mathrm{eq1}}} \right)}{R_0^2 V_{\mathrm{m1}}}} \cdot \exp\left(-\frac{\Delta E_{\mathrm{app1}}}{RT} \right) \cdot \frac{T - T_0}{\eta} \right]^3 - \alpha_2 \left[1 - \frac{K_0 P_{\mathrm{H_2}}}{R_0 V_{\mathrm{m2}}} \cdot \exp\left(-\frac{\Delta E_{\mathrm{app2}}}{RT} \right) \cdot \frac{T - T_0}{\eta} \right]^3 \quad (5)$$

where indices "1" and "2" refer to the first and second reactions, respectively; α_1 and $\alpha_2$are coefficients depending on the oxygen loss of each single reaction; K_0 and $K_{\mathrm{H}}^{0\beta}$ are temperature-independent constants; $P_{\mathrm{H_2}}$ is the hydrogen partial pressure; R and T are the gas constant and absolute temperature in Kelvin, respectively; T_0 is the initial temperature for reduction reaction; D_{H}^0 is the diffusion coefficient of hydrogen in the product layer; $P_{\mathrm{H_2}}^{\mathrm{eq1}}$ is the equilibrium hydrogen partial pressure at the reaction interface and should be related to T; $R_0$is the particle radius; V_{m1} and V_{m2} are coefficients that depend on substances and reactions; ΔE_{app1} and ΔE_{app2} are the apparent activation energies of the dual reactions. If the value of $P_{\mathrm{H_2}}^{\mathrm{eq1}}$ is very small or the temperature coefficient of $P_{\mathrm{H_2}}^{\mathrm{eq1}}$ can be neglected, then $\dfrac{2K_{\mathrm{H}}^{0\beta}D_{\mathrm{H}}^0\left(\sqrt{P_{\mathrm{H_2}}}-\sqrt{P_{\mathrm{H_2}}^{\mathrm{eq1}}}\right)}{{R_0}^2V_{\mathrm{m1}}}$ will be constant as the hydrogen partial pressure and the particle radius are fixed.

It should be noted that hydrogen diffusion is assumed to be the controlling step of the first reaction (Eq. (3)). However, water vapor diffusion in the product layer may also be the controlling step. In this case, the hydrogen diffusion resistance in the product layer can be neglected and the chemical reaction at the interface can be approximately considered to be in equilibrium. Therefore, water vapor partial pressure at the reaction interface can be calculated to be a linear function of hydrogen partial pressure at the interface that is equal to hydrogen partial pressure in the initially introduced gas. Thus, the kinetic formula for the case that water vapor diffusion in the product layer is the rate-controlling step should have a similar form to Eq. (5).

(a) Influences of temperature T and heating rate η.

Define

$$B_{T1}=\frac{1}{(2K_{\mathrm{H}}^{0\beta}D_{\mathrm{H}}^0/V_{\mathrm{m1}})\left(\sqrt{P_{\mathrm{H_2}}}-\sqrt{P_{\mathrm{H_2}}^{\mathrm{eq1}}}\right)/R_0^2} \tag{6}$$

$$B_{T2}=\frac{1}{(K_0/V_{\mathrm{m}})P_{\mathrm{H_2}}/R_0} \tag{7}$$

where B_T is a function of $P_{\mathrm{H_2}}$ and R_0, which will be constant when the hydrogen partial pressure and the particle size are fixed. Substituting Eqs. (6) and (7) into Eq. (5), Eq. (5) will become

$$\xi=1-\alpha_1\left[1-\sqrt{\frac{\exp\left(-\dfrac{\Delta E_{\mathrm{app1}}}{RT}\right)}{B_{T1}}\cdot\frac{T-T_0}{\eta}}\right]^3-\alpha_2\left[1-\frac{\exp\left(-\dfrac{\Delta E_{\mathrm{app2}}}{RT}\right)}{B_{T2}}\cdot\frac{T-T_0}{\eta}\right]^3 \tag{8}$$

(b) Influence of hydrogen partial pressure.

Define

$$B_{P1}=\frac{1}{(2K_{\mathrm{H}}^{0\beta}D_{\mathrm{H}}^0/V_{\mathrm{m1}})/R_0^2} \tag{9}$$

$$B_{P2}=\frac{1}{(K_0/V_{\mathrm{m2}})/R_0} \tag{10}$$

where B_P is a function of R_0. B_P will be constant as the particle size is fixed. Combining Eqs. (5), (9), and (10), one obtains

$$\xi=1-\alpha_1\left[1-\sqrt{\frac{\sqrt{P_{\mathrm{H_2}}}-\sqrt{P_{\mathrm{H_2}}^{\mathrm{eq1}}}}{B_{P1}}\exp\left(-\frac{\Delta E_{\mathrm{app1}}}{RT}\right)\cdot\frac{T-T_0}{\eta}}\right]^3-\alpha_2\left[1-\frac{P_{\mathrm{H_2}}}{B_{P2}}\exp\left(-\frac{\Delta E_{\mathrm{app2}}}{RT}\right)\cdot\frac{T-T_0}{\eta}\right]^3 \tag{11}$$

3.5.2 Application of the new model

Considering the small value of x (= 0.27) relative to 3 in TTM ($Fe_{3-x}Ti_xO_4$), which corresponds to the fractions of Fe_3O_4 and Fe_2TiO_4 in $Fe_{3-x}Ti_xO_4$, Fe_3O_4 reduction is dominated with respect to Fe_2TiO_4. Therefore, for simplicity, α_1 and α_2 will be approximately calculated according to Fe_3O_4 reduction: magnetite → wüstite and wüstite → iron. Thus, α_1 and α_2 are calculated to be 0.25 and 0.75, respectively. According to thermodynamics calculation, $P_{\mathrm{H_2}}^{\mathrm{eq}}$ is very small, so, in this study, $P_{\mathrm{H_2}}^{\mathrm{eq}}$ is neglected.

(a) Influences of temperature T and heating rate η.

Eq. (8) was used to fit the non-isothermal reduction curves of TTM. The fitting results are shown in Fig. 7, from which it can be seen that Eq. (8) can well describe experimental data, and the apparent activation energies of the first and second reactions were calculated to be

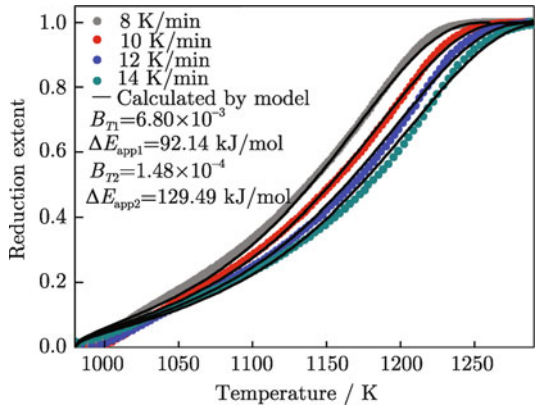

Fig. 7. Comparison between the measured and model estimated curves for non-isothermal reduction of TTM powders by pure H_2.

92.14 and 129.49 kJ/mol, respectively. The model describing non-isothermal reduction behavior of TTM by hydrogen is given as follows:

$$\xi = 1 - 0.25\left[1 - \sqrt{\frac{\exp\left(-\frac{92139.35635}{RT}\right)}{0.006798}\cdot\frac{T-T_0}{\eta}}\right]^3 - 0.75\left[1 - \frac{\exp\left(-\frac{129493.5793}{RT}\right)}{0.000148}\cdot\frac{T-T_0}{\eta}\right]^3 \quad (12)$$

(b) Influence of hydrogen partial pressure.

Based on Eq. (11), a cluster of theoretical curves has been calculated as shown in Fig. 8, from which it can be seen that most of the experimental points coincide with the theoretical predicted curves. Thus, the influence of hydrogen partial pressure on TTM reduction by hydrogen can be expressed as

$$\xi = 1-\alpha_1\left[1 - \sqrt{\frac{\sqrt{P_{H_2}}}{0.01264}\exp\left(-\frac{90279.58}{RT}\right)\cdot\frac{T-T_0}{10}}\right]^3 - \alpha_2\left[1 - \frac{P_{H_2}}{0.000114}\exp\left(-\frac{131923.9}{RT}\right)\cdot\frac{T-T_0}{10}\right]^3 \quad (13)$$

The comparison of parameters extracted in isothermal experiments [1] with those extracted in non-isothermal experiments in this study is listed in Table 3, from which it can be found that they are in good agreement.

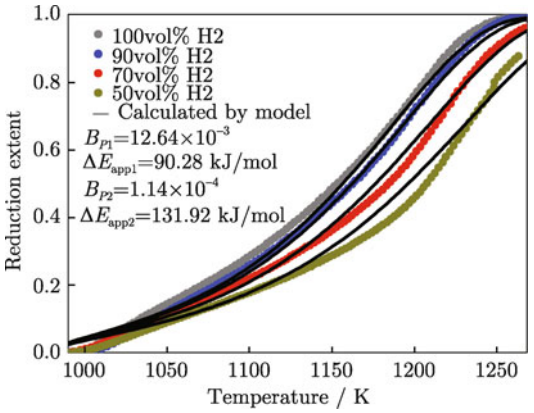

Fig. 8. Comparison between the measured and model estimated curves for non-isothermal reduction of TTM powders by H_2-Ar gas mixtures.

Table 3. Comparison of parameters extracted by the isothermal reduction model and the non-isothermal reduction model

Item	TTM→wüstite		wüstite→iron		Correlation coefficient
	B_{T1}/B_{P1}	ΔE_{app1}/(kJ·mol^{-1})	B_{T2}/B_{P2}	ΔE_{app2}/(kJ·mol^{-1})	
Isothermal reduction	3.71×10^{-3}	98.04	2.38×10^{-4}	115.06	0.995
Non-isothermal reduction (pure hydrogen)	6.80×10^{-3}	92.14	1.48×10^{-4}	129.49	0.999
Non-isothermal reduction (different hydrogen partial pressure)	12.64×10^{-3}	90.28	1.14×10^{-4}	131.92	0.997

4. Conclusions

(1) Increasing the heating rate can increase the reduction rate of TTM by hydrogen, and the maximum reduction rate appears at around 1200 K during the non-isothermal reduction process.

(2) The non-isothermal reduction of TTM by H_2 proceeds via a dual-reaction mechanism. The first reaction is reduction of TTM to wüstite and ilmenite and the second one is reduction of wüstite and ilmenite to iron and titanium dioxide.

(3) The present model can be applied to describe the non-isothermal reduction kinetics of TTM, and the predicted curves agree well with experimental results. According to this model, the rate-controlling steps for the first and second steps as well as kinetic parameters are obtained. The apparent activation energies are 90-98 and 115-132 kJ/mol for the first and second reactions, respectively.

Acknowledgements

The authors would like to acknowledge financial support from the National Natural Science Foundation of China (No. 11220158) and the Fundamental Research Funds for the Central Universities (FRF-TP-13-002A).

References

[1] J. Dang, X.J. Hu, G.H. Zhang, X.M. Hou, X.B. Yang, and K.C. Chou, Kinetics of reduction of titano-magnetite powder by H_2, *High Temp. Mater. Processes*, 32(2013), No. 3, p. 229.

[2] H.B. Zuo, Z.W. Hu, J.L. Zhang, J. Li, and Z.J. Liu, Direct reduction of iron ore by biomass char, *Int. J. Miner. Metall. Mater.*, 20(2013), No. 6, p. 514.

[3] G.D. McAdam, D.J. ÓBrien, and T. Marshall, Rapid reduction of New Zealand ironsands, *Ironmaking Steelmaking*, 4(1977), No. 1, p. 1.

[4] E. Park and O. Ostrovski, Reduction of titania-ferrous ore by carbon monoxide, *ISIJ Int.*, 43(2003), No. 9, p. 1316.

[5] A.A. Morozov, V.A. Reznichenko, A.Y. Sinadskii, and I.A. Karyazin, Metallurgical properties of titanomagnetite concentrate from the Kuril'sk Islands and its electromelted

slags, *Russ. Metall.*, 4(1998), No. 2, p. 3.

[6] J.M. Pang, P.M. Guo, P. Zhao, C.Z. Cao, D.G. Zhao, and D.G. Wang, Reduction of 1-3 mm iron ore by H_2 in a fluidized bed, *Int. J. Miner. Metall. Mater.*, 16(2009), No. 6, p. 620.

[7] Y.J. Wang and K.G. Zhou, Preparation of spherical ultrafine copper powder via hydrogen reduction-densification of $Mg(OH)_2$-coated Cu_2O powder, *Int. J. Miner. Metall. Mater.*, 19(2012), No. 11, p. 1063.

[8] Y.J. Xin, Z.M. Guo, J. Luo, R.X. Wang, and Z.C. Fang, Preparation of coarse and spherical tungsten powders by ammonium paratungstate, *J. Univ. Sci. Technol. Beijing*, 35(2013), No. 3, p. 352.

[9] X.G. Si, X.G. Lu, C.W. Li, C.H. Li, and W.Z. Ding, Phase transformation and reduction kinetics during the hydrogen reduction of ilmenite concentrate, *Int. J. Miner. Metall. Mater.*, 19(2012), No. 5, p. 384.

[10] Y.M. Wang, Z.F. Yuan, H. Matsuura, and F. Tsukihashi, Reduction extraction kinetics of titania and iron from an ilmenite by H_2-Ar gas mixtures, *ISIJ Int.*, 49(2009), No. 2, p. 164.

[11] K. Sun, T. Akiyama, R. Takahashi, and J.I. Yagi, Hydrogen reduction of natural ilmenite in a fluidized bed, *ISIJ Int.*, 35(1995), No. 4, p. 360.

[12] R.A. Briggs and A. Sacco, Hydrogen reduction mechanisms of ilmenite between 823 and 1353 K, *J. Mater. Res.*, 6(1991), No. 3, p. 574.

[13] E. Park and O. Ostrovski, Reduction of titania-ferrous ore by hydrogen, *ISIJ Int.*, 44(2004), No. 6, p. 999.

[14] W.K. Jozwiak, E. Kaczmarek, T.P. Maniecki, W. Ignaczak, and W. Maniukiewicz, Reduction behavior of iron oxides in hydrogen and carbon monoxide atmospheres, *Appl. Catal., A*, 326(2007), No. 1, p. 17.

[15] J. Dang, K.C. Chou, X.J. Hu, and G.H. Zhang, Reduction kinetics of metal oxides by hydrogen, *Steel Res. Int.*, 84(2013), No. 6, p. 526.

[16] K.C. Chou, A kinetic model for oxidation of Si-Al-O-N materials, *J. Am. Ceram. Soc.*, 89(2006), No. 5, p. 1568.